Symmetry-Forbidden vs Symmetry-Allowed Electron and Hole Transfer in Medium Sized Intramolecular Organic Donor−Acceptor Radical Ions. A Trajectory Surface Hopping Study

Garth A. Jones and Michael N. Paddon-Row*

School of Chemistry, University of New South Wales, Sydney 2052, Australia

Barry K. Carpenter

Department of Chemistry and Chemical Biology, Baker Laboratory, Cornell University, Ithaca, New York 14853-1301

Piotr Piotrowiak

Department of Chemistry, Rutgers University, Newark, New Jersey 07102

Received: January 31, 2002; In Final Form: March 20, 2002

This paper presents a quasi-classical molecular dynamics study of symmetry effects on the dynamics of intramolecular electron transfer and hole transfer in a series of rigid organic donor−acceptor radical ions derived from **3** − **8**, in which pairs of identical chromophores (double bonds, cyclopentadiene groups, or fulvene units) are attached to opposite ends of either an adamantane bridge or a bishomocubane bridge. The charge-shift process taking place by the most symmetrical transition structure in the mono-radical ions of these species may be either formally symmetry-allowed or symmetry-forbidden, depending on the sign of the migrating charge, the nature of the chromophore pair, and the identity of the connecting bridge. The degree to which symmetry breaking molecular vibrations affect the dynamics of charge-shift in these systems was explored using a recently developed Landau−Zener trajectory surface hopping (LZ-TSH) model. Reaction trajectories, which may hop between the ground state and the first excited state potential energy surface, of the radical ions were calculated "on the fly" using the AM1-CI theoretical model. Canonical ensembles of approximately 200 trajectories were used to calculate frequencies of passage for the charge-shift processes in the radical ions of **3**−**8**. It was found that frequencies of passage for the formally symmetry-forbidden charge-shift processes were only marginally smaller than those for the corresponding formally symmetry-allowed processes, implying that symmetry breaking vibrational modes are playing an important role in the charge-transfer dynamics of these systems. The identification of these symmetry breaking modes was secured by calculating secondary kinetic isotope effects and by carrying out Fourier transform analyses of reaction trajectories. Our conclusion concerning the weak role played by symmetry effects on the dynamics of charge migration processes receives support from some published experimental data.

I. Introduction

Traditionally, charge transfer (CT) processes are described by the mixing of two diabatic surfaces, one representing the electronic configuration of the reactant, the other the configuration of the product. In regions where the diabatic surfaces approach each other, mixing may occur, giving rise to an avoided crossing. At these points in the potential energy surface (PES), the magnitude of the diabatic coupling is equal to half the energy gap between the two adiabatic surfaces (ΔE_{ac}). In the weak coupling limit, the rate of electron transfer (ET) or hole transfer (HT) may be obtained by the Fermi golden rule (FGR), where the rate of ET k_{et} is related to the electronic coupling, V_{el} and the Franck−Condon weighted density of states, $\{FCWD\}$, by eq 1

$$k_{et} = \frac{4\pi^2}{h}|V_{el}|^2\{\mathrm{FCWD}\} \qquad (1)$$

The magnitude of both V_{el} and FCWD are highly dependent on environmental factors. Thus, it has been well established in many experimental studies that intramolecular electron transfer and hole transfer occurring in multichromophoric systems depend on, among other things, the distance between the chromophores,[1−5] the orientation of the chromophores with respect to each other and with the bridge,[6] solvent effects,[7,8] and the driving force of the reaction.[9,10] Of particular interest to the current study is the effect of orbital symmetry on ET and HT processes.[11−14]

Photoinduced intramolecular ET has been observed to occur in systems where it is formally forbidden on the grounds of state symmetry. Two examples are given below. ET in **1** occurs from the locally excited singlet state of the dimethoxynaphthalene (DMN) donor to the dicyanovinyl (DCV) acceptor. Within the context of C_s symmetry, the lowest excited state of **1** has A′ symmetry, whereas the charge separated product state has A″ symmetry. The electronic coupling for the ET process under these constraints in therefore zero.

The electronic coupling for photoinduced ET in **2** should likewise be zero, if this system retains local D_{2d} symmetry in the bismethyleneadamentane unit. Nevertheless, rapid ET is observed to occur in both **1** and **2** at rates greater than 10^8

* To whom correspondence should be addressed. E-mail: m.paddonrow@unsw.edu.au.

10.1021/jp0255839 CCC: $22.00
Published on Web 04/17/2002

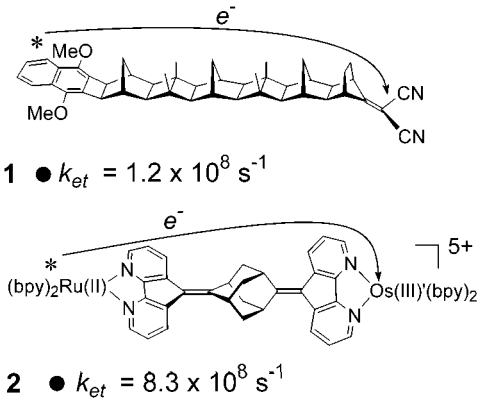

s^{-1}.[13−15] The rapid rates of ET occurring in these systems may be explained in terms of vibronic coupling. That is, molecular vibrations remove the symmetry constraints, thereby allowing V_{el} to take on a finite magnitude.

Similar symmetry considerations apply to excitation energy transfer processes, in which the donor−acceptor electronic interactions are governed by two-electron four-orbital exchange and Coulomb integrals. Strong symmetry control of energy transfer was demonstrated in degenerate and nearly degenerate bichromophoric spiranes in a supersonic jet.[16] However, under identical conditions, rapid formally symmetry-forbidden electronic excitation transfer (> 10^{12} s^{-1}) was observed in closely related orthogonal spiranes with larger donor−acceptor energy gaps. This behavior has also been explained in terms of vibronic coupling.[17]

Questions which arise from these experimental data include: What vibrational modes are responsible for generating the electronic coupling required for rapid ET to occur in these systems? How important are the bridge vibrations compared to the chromophore vibrations in determining the magnitude of V_{el}?

Answers to these questions can be obtained by performing trajectory simulations, on model systems, which explicitly include the effects of molecular vibrations. In the current study, this is done with the use of a recently developed semiempirical molecular dynamics model which incorporates a Landau−Zener[18,19] based trajectory surface hopping[20−23] model (LZ-TSH). Application of the LZ-TSH algorithm involves running approximately 200 quasi-classical trajectories for each of the systems considered, and calculating a frequency of passage (*f*) for the ET or HT process of interest. Details of the method are described in two previous papers.[24,25] An overview of the LZ-TSH methodology is also presented in Appendix A of this paper.

In this paper, the LZ-TSH model is used to investigate the effects of molecular vibrations on the dynamics of ET and HT processes in formally orbital symmetry-forbidden charge-shift processes in a series of judiciously designed anion and cation radicals, **3**−**8**. In their most symmetrical structures, **3**, **5**, and **7**, which contain the adamantane bridge, have D_{2d} symmetry, and **4**, **6**, and **8**, which possess the bishomocubane bridge, all have D_{2h} symmetry.

HT is investigated in cation radicals $\mathbf{3}^+$ and $\mathbf{4}^+$, whereas both HT and ET are investigated in the respective cation and anion radicals of $\mathbf{5}^{\pm}$, $\mathbf{6}^{\pm}$, $\mathbf{7}^{\pm}$ and $\mathbf{8}^{\pm}$.[26] Approximate secondary kinetic isotope effects are calculated for $\mathbf{3}^+$ and $\mathbf{4}^+$ to help determine the effect of the magnitude of the frequencies of the symmetry-breaking vibrations on the frequencies of passage for the charge-shift processes.

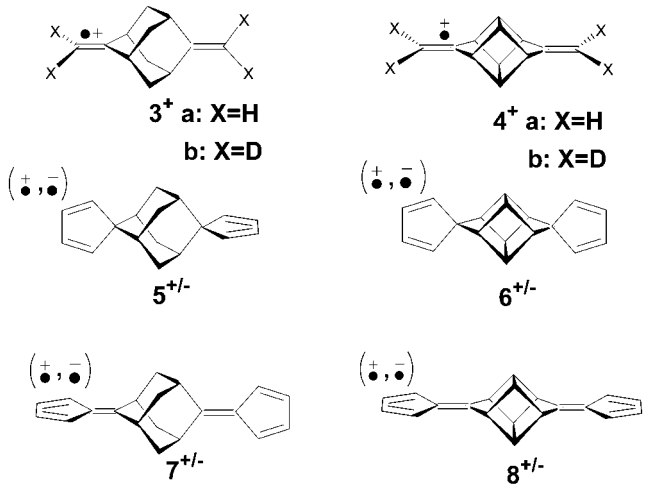

This paper is arranged along the following lines. The computational details are given in section II, and the qualitative details of the systems of interest are given in section III. The potential energy surface (PES) information for all systems are given in section IV, and the trajectory surface hopping results are presented in section V. Finally, section VI provides a summary and conclusions of this study.

II. Computational Details

The Landau−Zener based trajectory surface hopping (LZ-TSH) model used in this study involves the running of semiempirical direct-dynamics trajectories, as implemented in MOPAC93,[27] on the systems of interest. Surface hopping (vertical electronic transitions) is allowed within the context of the Landau−Zener approximation, and may occur at avoided crossings only.

For each of the radical ions considered here, accurate representations of the full adiabatic potential energy surfaces would reveal the existence of a 3N-8 dimensional seam of intersection between them. Encounter of this seam would be dynamically important but statistically improbable because it requires that two characteristic coordinates (the gradient difference and the nonadiabatic coupling coordinates) simultaneously have specific values.[28] In the trajectory calculations described here, the probability of satisfying that criterion during the (maximum) 500 fs of a typical run is negligible. When the system is displaced from the seam of intersection along either of the characteristic coordinates, the potential energy surfaces experience avoided crossings.[28] Consequently, the use of an avoided-crossing model in the estimation of surface-hop probabilities seems appropriate.

Ensembles of approximately 200 individual trajectories are run for each of the systems of interest. Each trajectory is terminated either when it enters the product well, and charge-shift is deemed to have occurred, or after 500 fs if charge-shift has not occurred in that time. The lifetime of each trajectory is recorded and the decay data for the charge-shift (CS) reactions (i.e., the fraction of trajectories, *F*, yet to have undergone CS after a time *t*, against time, *t*) are analyzed by fitting monoexponential decay functions to them. The frequencies of passage (*f*) are then calculated for each of the charge-shift processes considered.[29] The canonical ensembles of trajectories are initialized at 298.15 K, using a quasi-classical normal-mode sampling procedure modified from that of Chapman and Bunker.[30] Details of the initialization procedure can be found in Appendix B of this paper.

The LZ-TSH model employs the "half-electron" approximation implemented in MOPAC93. The AM1-CI method with its original parameters are used for the trajectories of systems $\mathbf{3}^+$, $\mathbf{4}^+$, $\mathbf{5}^\pm$, $\mathbf{6}^\pm$, $\mathbf{7}^+$, and $\mathbf{8}^+$. Because of the technical difficulties which were encountered using the AM1 level for calculations of anion radicals $\mathbf{7}^-$ and $\mathbf{8}^-$, the PM3 model with its original parameters was used in these cases.

The active space chosen for each of the systems was a minimal 2×2 CI. In the case of the cation radicals, this comprised three electrons and two orbitals (the HOMO and HOMO-1), and for the anion radicals it comprised one electron in two orbitals (the SOMO and LUMO). Tests were preformed which involved running LZ-TSH dynamics calculations on the biscyclopentadiene (**5** and **6**) and bisfulvene (**7** and **8**) systems using a larger CI active space (7 electrons in 8 orbitals for $\mathbf{5}^+$ and $\mathbf{6}^+$ and 11 electrons in 12 orbitals for $\mathbf{7}^+$ and $\mathbf{8}^+$). Results obtained using the larger CI spaces were essentially the same as those using the minimal 2×2 active space. Consequently, all results presented in this paper were obtained using the minimal 2×2 CI method in order to reduce the amount of CPU time required to run the ensembles of 200 trajectories.

Because, within the context of the LZ criterion, the probability of trajectory surface hopping is related to the square of the coupling matrix element V_{el}, the rate of fluctuation of the energy gap, ΔE between the ground state and the first excited state as the trajectory progresses should give an indication of the rate at which the avoided crossing is encountered and, therefore, an indication of the rate of charge transfer. To delineate which molecular vibrations are important contributors to the energy gap fluctuation, a single trajectory for some of the systems was run and a Fourier transform (FT) of ΔE versus t was taken to give intensity (arbitrary units) versus frequency (cm^{-1}). Throughout this paper, the energy gap corresponding to the highest symmetry, charge-delocalized structure is defined as ΔE_{ac}.

Legitimate criticism may be leveled against using our Landau−Zener based TSH model, together with AM1-CI to calculate the potential energy surfaces, for calculating *quantitatively* the dynamics of charge migration processes. However, in this study, we are interested only in *qualitative* trends which lead to useful insights into identifying factors which play prominent roles in modulating the dynamics of charge migration reactions. In this context, our methodology is adequate and has been justified in previous publications in this series.[24,25]

III. Systems of Interest

The chromophores in **3**, **5**, and **7** are separated by an adamantane bridge, 3.4 Å in length, and those in **4**, **6**, and **8** are separated by a bishomocubane bridge 4.0 Å in length. It is likely that the origin of any interchromophoric electronic coupling in **3**-**8** is predominantly through-bond in character,[31,32] reinforced by a smaller through-space contribution. In this context, it is important to note that both adamantane and bishomocubane bridges possess the same number (four) of main coupling relays of σ-bonds connecting the chromophores, each relay possessing four σ-bonds. Putting orbital symmetry effects aside, for the moment, the above analysis indicates that through-bond electronic coupling has comparable magnitudes in both types of bridge. The bridges, therefore, are ideal frameworks for exploring orbital symmetry effects on the dynamics of processes that are dependent on electronic coupling, such as ET and energy transfer.

The effect of orbital symmetry on the magnitude of the electronic coupling element, V_{el}, for HT and ET in $\mathbf{3}^\pm - \mathbf{8}^\pm$ may be easily deduced by remembering that, within the context of Koopmans' theorem, the active orbitals of the chromophores that are involved in HT are derived from the two (localized) HOMOs, one from each chromophore. Likewise, the two active orbitals involved in ET are derived from the pair of (localized) LUMOs, one from each chromophore.

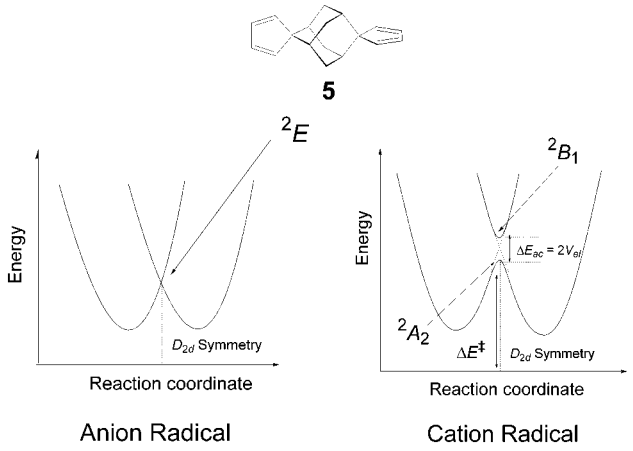

Figure 1. Schematics of the transition structures of the anion and cation radicals of **5** at D_{2d} symmetry. Electron transfer in $\mathbf{5}^-$ is formally symmetry-forbidden, but HT in $\mathbf{5}^+$ is formally symmetry-allowed.

Application of this knowledge to **3**−**8** leads to the following predictions. For the systems possessing the bishomocubane bridge ($\mathbf{4}^+$, $\mathbf{6}^\pm$, and $\mathbf{8}^\pm$), and which are constrained to adopt D_{2h} symmetry, the two chromophore HOMOs have the same symmetry, as do the two chromophore LUMOs. Consequently, mixing of the HOMOs leads to a nonzero value for the interchromophore electronic coupling for HT, and mixing of the two LUMOs leads to a nonzero value of V_{el} for ET. Thus, both ET and HT are symmetry-allowed processes in the bishomocubane bridge systems.

In some of the adamantane-based systems, however, the electronic coupling may be 'switched-off′ by the orbital symmetries when their molecular geometries possess maximum symmetry (D_{2d}). The two localized double bond HOMOs in D_{2d} **3** are unable to mix, because they have different local symmetries.

Thus, for HT in $\mathbf{3}^+$, proceeding via a D_{2d} symmetry transition structure, the active configurations have ^2E symmetry and V_{el} is therefore zero. Hole transfer in $\mathbf{3}^+$ is therefore a formally symmetry-forbidden process. Although ET in the analogous anion radical of **3**, is not considered in this investigation, the same kind of analysis shows that ET is also symmetry-forbidden in this system.

In the case of the D_{2d} biscyclopentadieneadamantane (BCA) **5**, the degeneracy of the two localized HOMOs is lifted (they have the same local symmetries) as a result of spiroconjugation.[33,34] This mixing leads to a nonzero value of V_{el} and HT in $\mathbf{5}^+$ proceeding via a D_{2d} transition state is symmetry-allowed. In contrast, the two localized chromophore LUMOs in D_{2d} **5** cannot mix, on the grounds of symmetry. Consequently, ET in $\mathbf{5}^-$, proceeding via the D_{2d} transition structure is symmetry-forbidden.

Figure 1 schematically displays the symmetry-forbidden nature of ET in $\mathbf{5}^-$, and the symmetry-allowed nature of HT in $\mathbf{5}^+$, at D_{2d} symmetry. The activation barrier ($\Delta E^\ddagger$) and energy gap at the avoided crossing ($\Delta E_{ac} = 2V_{el}$) are also displayed.

Application of a similar type of analysis to the D_{2d} bisfulveneadamantane systems, $\mathbf{7}^+$ and $\mathbf{7}^-$ leads to the prediction that hole transfer in $\mathbf{7}^+$ is formally symmetry-allowed, as a result of spiroconjugation between the fulvene units, whereas ET in $\mathbf{7}^-$ is formally symmetry-forbidden.

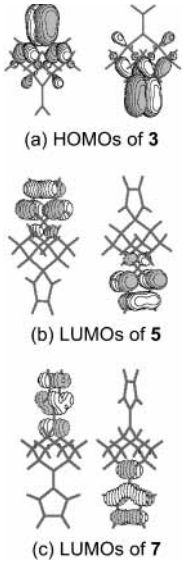

Figure 2. Degenerate HOMOs of **3** and degenerate LUMOs of **5** and **7**. Hole transfer in the cation radical of **3**, and ET in the anion radicals of **5** and **7** are formally forbidden on the basis of state symmetry.

In summary, the bishomocubane based systems possess D_{2h} symmetry for their most symmetric transition structures, and all of these transition structures are associated with finite energy gaps between the active configurations involved in the charge-shift reactions. Consequently, charge-shift is a formally symmetry-allowed event for all of these systems. In the case of the adamantane based systems, their most symmetric transition structures have D_{2d} symmetry, and charge-shift may be either symmetry-allowed or symmetry-forbidden, depending on which orbitals are involved. If a reaction trajectory for $\mathbf{3}^+$ passes through a D_{2d} transition structure, then HT should not occur, and this is also the case for electron transfer in $\mathbf{5}^-$ and $\mathbf{7}^-$. However, spiroconjugative coupling occurs in $\mathbf{5}^+$ and $\mathbf{7}^+$, and this makes HT a symmetry-allowed event, even if a reaction trajectory proceeds via a D_{2d} transition structure. The AM1 degenerate HOMOs of **3** and degenerate LUMOs of **5** and **7** are displayed in Figure 2, and the (nondegenerate) HOMO and HOMO-1, resulting from spiroconjugation, of **5** and **7** are shown in Figure 3.

IV. Potential Energy Surfaces of the Systems

The potential energy surface characterization and dynamics calculations for $\mathbf{3}^+$, $\mathbf{4}^+$, $\mathbf{5}^\pm$, $\mathbf{6}^\pm$, $\mathbf{7}^+$, and $\mathbf{8}^+$, were performed at the AM1 level, with a 2×2 CI (AM1-CI) which is composed of three electron occupying the two $\pi-$orbitals. The two orbitals making the active space of the CI are the orbitals associated with the charge-shift processes for each of the systems considered. The PES and dynamics calculations for the bisfulvene anion radicals, $\mathbf{7}^-$ and $\mathbf{8}^-$, were performed using the semiempirical PM3 Hamiltonian. This is because all attempts to locate the AM1-CI charge localized structures failed. All optimization attempts resulted in either, the fully symmetric charge-delocalized structure, or a charge-localized structure with at least two large imaginary frequencies.

It is now relatively common for direct-dynamics calculations on polyatomic systems to use semiempirical MO methods that have been reparametrized to fit ab initio results at the key stationary points.[35−38] In the present case, the use of this approach was precluded by the difficulty of finding a computationally tractable ab initio model that could adequately describe the radical ions being studied.

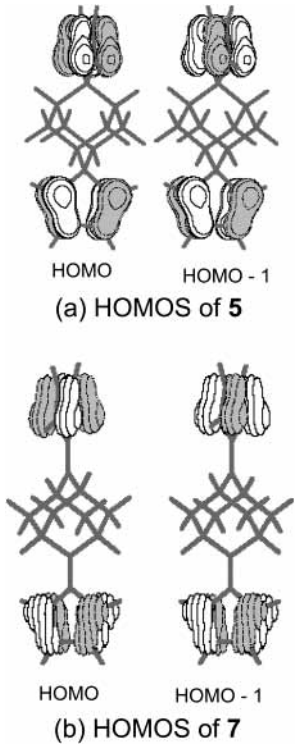

Figure 3. HOMO and HOMO-1 of **5** and **7**. Here the degeneracy has been lifted by spiroconjugation. HT in these systems is formally symmetry-allowed.

TABLE 1: Summary of the $\Delta E^\ddagger$ and ΔE_{ac} Values

ion	symmetry (deloc)	symmetry (loc)	$\Delta E^\ddagger$	ΔE_{ac}
$\mathbf{3a}^+$ (SF)[a]	D_{2d}	C_1	3.1	0.0
$\mathbf{3b}^+$ (SF)	D_{2d}	C_1	3.1	0.0
$\mathbf{4a}^+$ (SA)[b]	D_{2h}	C_1	0.7	6.5
$\mathbf{4b}^+$ (SA)	D_{2h}	C_1	0.7	6.5
$\mathbf{5}^+$ (SC)[c]	D_{2d}	C_{2v}	3.1	0.75
$\mathbf{6}^+$ (SA)	D_{2h}	C_{2v}	3.4	0.55
$\mathbf{7}^+$ (SC)	D_{2d}	C_{2v}	4.5	6.8×10^{-3}
$\mathbf{8}^+$ (SA)	D_{2h}	C_{2v}	4.5	1.6×10^{-3}
$\mathbf{5}^-$ (SF)	D_{2d}	C_{2v}	1.3	0.00
$\mathbf{6}^-$ (SA)	D_{2h}	C_{2v}	0.2	2.8
$\mathbf{7}^-$ (SF)	D_{2d}	C_{2v}	1.7	0.0
$\mathbf{8}^-$ (SA)	D_{2h}	C_{2v}	2.2	4.3

All energies are in kcal mol^{-1}. [a] The charge-shift reaction is a symmetry-forbidden (SF) event in these systems. [b] The charge-shift reaction is symmetry-allowed (SA) in these systems. [c] Spiroconjugation (SC) occurs in these systems.

For all systems considered, the fully symmetric (D_{2d} and D_{2h}), charge-delocalized structures lay higher in energy than the lower symmetry, charge-localized structures. The charge-localized structures of $\mathbf{3}^+$ and $\mathbf{4}^+$ possess C_1 symmetry, with the positive charge formally localized on one of the double bonds, making those double bonds essentially one-electron $\pi-$bonds. These one-electron $\pi-$bonds are twisted about their internuclear axes, by 22.5° for $\mathbf{3}^+$ and 25.4° for $\mathbf{4}^+$. This is consistent with the fact that the ethylene cation radical has been shown, both experimentally and computationally, to exhibit a similar degree of torsion.[39−43] All of the charge-localized structures of the biscyclopentadiene and bisfulvene systems have C_{2v} symmetries.

Table 1 displays the data for the relevant stationary points on the PESs for HT and ET, including the maximum symmetries of the charge-localized and charge-delocalized structures, the activation barriers ($\Delta E^\ddagger$), and the energy gaps (ΔE_{ac}) at the optimized, highest symmetry geometries for each of the systems (see Figure 1).

TABLE 2: Important Data of All Systems Studied in This Study Using the LZ-TSH Model. All Energies Are in Kcal Mol^{-1}

ion	$\Delta E^{\ddagger}$	ΔE_{ac}	f (s^{-1})	rms	relative f
3a$^+$ (SF)[a]	3.1	0.00	9.57×10^{12}	0.046	2.7
3b$^+$ (SF)	3.1	0.00	7.01×10^{12}	0.021	2.0
4a$^+$ (SA)[b]	0.7	6.5	1.55×10^{13}	0.033	4.4
4b$^+$ (SA)	0.7	6.5	1.34×10^{13}	0.029	3.8
5$^+$ (SC)[c]	3.1	0.75	1.49×10^{13}	0.009	4.2
6$^+$ (SA)	3.4	0.55	7.08×10^{12}	0.048	2.0
7$^+$ (SC)	4.5	6.8×10^{-3}	3.55×10^{12}	0.025	1
8$^+$ (SA)	4.5	1.55×10^{-3}	4.79×10^{12}	0.019	1.3
5$^-$ (SF)	1.3	0.00	1.71×10^{13}	0.015	4.8
6$^-$ (SA)	0.2	2.4	6.78×10^{13}	0.017	19.1
7$^-$ (SF)	1.7	0.0	1.55×10^{13}	0.014	4.4
8$^-$ (SA)	2.2	4.3	5.28×10^{13}	0.016	14.8

[a] The charge-shift reaction is a symmetry-forbidden (SF) event in these systems. [b] The charge-shift reaction is symmetry-allowed (SA) in these systems. [c] Spiroconjugation (SC) occurs in these systems.

Recent ab initio calculations have been carried out on stationary points of **3**$^+$ at the CASSCF(3,4)/3-21G* level.[44] The charge-localized C_{2v}-symmetry structure was found to lie 3.4 kcal mol^{-1} lower in energy than the optimsed D_{2d}-symmetry, charge-delocalized structure. This is in qualitative agreement with our AM1-CI calculations, where the C_1 charge-localized structure is 3.1 kcal mol^{-1} lower in energy than the D_{2d} charge-delocalized structure.

At 298 K, the majority trajectories should possess sufficient kinetic energy to overcome the activation barriers for all charge-shift reactions considered. ET and HT processes are generally considered to be adiabatic when $V_{el} > k_B T \cong 0.6$ kcal mol^{-1}, at 298.15 K.[45] Consequently, surface hopping is expected to occur readily for all ensembles, except **4**$^+$, **6**$^-$, and **8**$^-$ whose ΔE_{ac} values exceed 1.2 kcal mol^{-1}.

V. The LZ-TSH Calculations

In this section, the LZ-TSH results are presented and analyzed. Hole transfer is a formally symmetry-forbidden process for some of the systems (**3**$^+$, **5**$^-$, and **7**$^-$), while it is formally allowed for the others. The prediction is that the formally symmetry-forbidden processes should be influenced by symmetry breaking vibrations more markedly than the formally symmetry-allowed processes. Table 2 summarizes the frequency of passage (f) data for the CS reactions. The root-mean-square values of the monoexponential fits (rms) and relative frequencies of passage are also displayed.

Although HT in **3**$^+$ is symmetry-forbidden if it proceeds via the D_{2d} charge-delocalized state, the LZ-TSH model predicts that very rapid intramolecular HT shoul take place in **3a**$^+$ with a frequency of passage of 9.57×10^{12} s^{-1}. Charge-shift reactions which are symmetry-forbidden have been previously attributed to vibronic coupling.[11,46] Our molecular dynamics calculations support this explanation. Thus, we find that the majority of trajectories for **3**$^+$ arriving at the transition region (avoided crossing) of the PES, have structures that are significantly distorted from D_{2d} symmetry. These structural distortions are manifestations of symmetry-breaking vibrational modes. Electronic coupling between the two diabatic configurations in these structurally unsymmetrical parts of the avoided crossing region lead to a finite energy gaps, ΔE_{ac} ($=2V_{el}$). Within the context of the LZ approach, the frequency of passage through the avoided crossing should increase with increasing magnitude of ΔE_{ac}. That is, fewer trajectories undergo surface hopping.

To identify which normal vibrational modes are the most important contributors to fluctuations of ΔE as a function of time, a single trajectory[47] for each system, **3a**$^+$ and **3b**$^+$ was run and the Fourier transform (FT) of ΔE versus t, for each trajectory, was taken to give intensity (arbitrary units) versus frequency (cm^{-1}). The FT spectrum for **3a**$^+$, shown in Figure 4, displays four major peaks at, 224, 1384, 1670, and 1893 cm^{-1}. These peaks were correlated with calculated normal harmonic vibrational modes (ν_h) for the optimized ground-state structure of **3a**$^+$. Thus, the peaks at 1670 and 1893 cm^{-1} are assigned, respectively, to the stretching modes of the charge-localized, one-electron $\pi-$bond ($\nu_h = 1659$ cm^{-1}) and the neutral two-electron π bond ($\nu_h = 1894$ cm^{-1}). The third most intense peak at 224 cm^{-1} corresponds to the torsional mode of the terminal CH_2 group about the charge-localized one-electron $\pi-$bond ($\nu_h = 235$ cm^{-1}). The peak at 1384 cm^{-1} probably corresponds to CH wagging distortions of the CH_2 groups and/or breathing modes of hydrocarbon cage. However, because of the high density of normal vibrational modes around this frequency, it was impossible to identify the exact mode responsible for this peak. Nevertheless, this peak is much less intense than the others and therefore the vibrational modes responsible for its appearance in the FT spectrum play little, if any role in bringing the trajectory to the avoided crossing.

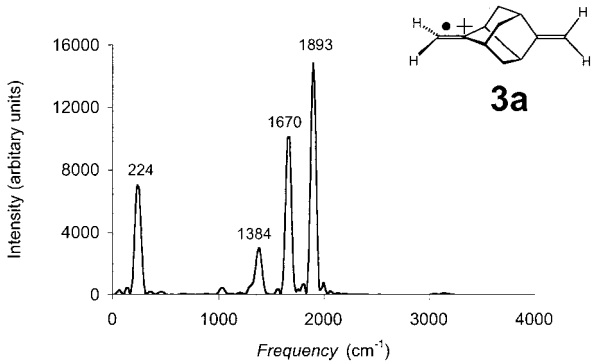

Figure 4. Fourier transform spectrum obtained from the ΔE versus time curve for **3a**$^+$, from a trajectory restricted to the reactant well. Four major peaks occur at 224, 1384, 1670, and 1893 cm^{-1}.

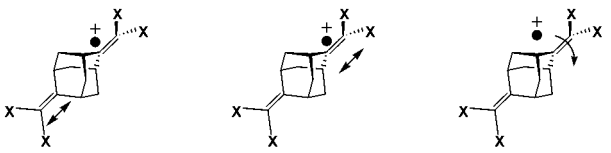

Figure 5. Three vibrational modes of **3a**$^+$, corresponding to the most intense peaks shown in the FT spectrum in Figure 4. The corresponding vibrational frequencies of the deuterated system, **3b**$^+$ are also displayed.

An FT spectrum for the deuterated species **3b**$^+$ displays three main peaks at 163, 1649 and 1873 cm^{-1}.[25] These correspond to the torsional mode ($\nu_d = 167$ cm^{-1}) and the two π bond stretching modes ($\nu_d = 1644$ and 1860 cm^{-1}). A fourth minor peak occurring at about 1000 cm^{-1} probably corresponds to the peak at 1384 cm^{-1} in the FT spectrum for **3a**$^+$. The relative intensity of this peak with respect to the other three in the FT spectrum for **3b**$^+$ indicates that replacing the methylene protons with deuterium reduces the significance of the effects of the CH/CD bending distortions to such a point that they barely contribute to the modulation of ΔE. Figure 5 displays the three vibrational modes corresponding to the three most intense peaks of the FT spectra of **3a**$^+$ and **3b**$^+$.

The LZ-TSH calculations provide insight into the role played by nuclear vibrations on the dynamics of HT in **3a**$^+$ and **3b**$^+$.

Comparing the frequencies of passage calculated from the LZ-TSH simulations for $\mathbf{3a}^+$ and $\mathbf{3b}^+$, it is predicted that HT should occur more rapidly in the former system as a consequence of a secondary kinetic isotope effect. An approximate secondary kinetic isotope effect (for **3a**:**3b**) can therefore be calculated

$$\frac{f(3\mathbf{a}^+)}{f(3\mathbf{b}^+)} = \frac{k_h}{k_d} \qquad (2)$$

The SKIE calculated for the HT reaction of $\mathbf{3a}^+$ is 1.37.

The role played by molecular vibrations in the HT processes for $\mathbf{3a}^+$ and $\mathbf{3b}^+$, can be better understood by considering the ratios of the magnitudes of the various vibrational frequencies of $\mathbf{3a}^+$ and $\mathbf{3b}^+$, in the FT spectra which are responsible for driving the trajectory to the avoided crossing. The ratios of the magnitudes of the π bond stretching frequencies for $\mathbf{3a}^+$:$\mathbf{3b}^+$ are small: 1.02 (= 1894 cm^{-1}/1860 cm^{-1}) for the two-electron $\pi-$bond stretching mode, and 1.01 (= 1659 cm^{-1}/1644 cm^{-1}) for the one-electron $\pi-$bond stretching mode. The ratio of the CX_2 torsional modes about the one-electron $\pi-$bond for $\mathbf{3a}^+$:$\mathbf{3b}^+$ is significantly larger at 1.41 (= 235 cm^{-1}/167 cm^{-1}). The similarity of this ratio to that of the SKIE ($k_h/k_d = 1.37$) indicates that the isotope effect is due largely to the torsional mode, and not the double bond stretching vibrations.[48]

The FT spectra for $\mathbf{3a}^+$ and $\mathbf{3b}^+$ indicate that there are two types of vibrational modes which are primarily responsible for driving the HT process, namely the stretching modes of the $\pi-$bonds and the CX_2 torsional mode about the one-electron $\pi-$bond. It is intuitively obvious that the $\pi-$bond stretching modes will be of primary importance in driving the trajectories to the charge-delocalized region of the PES, which corresponds to the transition state for the HT process. This is because the lengths of the two double bonds must approach each other for the charge to delocalize over both chromophores. In fact, Robb et. al. have shown that the antisymmetric combination of $\pi-$bond stretching modes corresponds to the charge-shift vector for the BMA cation radical, $\mathbf{3}^+$, at the CASSCF(3,4)/3-21G level of theory.[44]

Although the $\pi-$bond stretches are necessary for driving the trajectories to the transition structure for the HT reaction, and bringing about delocalization of the excess positive charge on the cation radical, these modes, in themselves, are not sufficient to induce HT. The avoided crossing must be associated with a finite V_{el} for HT to occur. The adiabatic regime for electron transfer is generally accepted to be defined when $V_{el} > k_BT \cong$ 0.6 kcal mol^{-1} at 298.15 K.[45] The torsional mode associated with the one-electron $\pi-$bond is therefore an essential part of the HT process. The $\pi-$bond stretching modes drive the trajectories from the reactant well to the charge-delocalized transition structure, and the torsional mode allows V_{el} to take on a finite value. Presumably the reason this mode is the dominant symmetry breaking mode is that this mode is responsible for maximizing the through-bond coupling, by overlap of the π-orbital of the one-electron double bond with the σ-orbitals of the adamantane bridge.

Because HT is formally symmetry-allowed in $\mathbf{4}^+$, the existence of symmetry breaking modes is not strictly necessary to permit HT to take place. Based on this fact, the LZ-TSH model is expected to predict a faster frequency of passage for HT in $\mathbf{4}^+$, than for $\mathbf{3}^+$. The LZ-TSH model does, in fact, predict intramolecular HT to be slightly faster in $\mathbf{4}^+$ than in $\mathbf{3}^+$, by a factor of 1.62, and 1.92 times faster in $\mathbf{4b}^+$, compared to $\mathbf{3b}^+$.

The calculated SKIE for HT in the bishomocubane cation radicals, $\mathbf{4a}^+$:$\mathbf{4b}^+$ is 1.15, which is noticeably smaller than the SKIE value of 1.37 for HT in $\mathbf{3a}^+$:$\mathbf{3b}^+$. The ratio of the frequencies (from the harmonic frequency calculation) of the CX_2 torsional vibrational modes about the one-electron π bond for the BMH cation radicals, $\mathbf{4a}^+$:$\mathbf{4b}^+$, is ν_h/ν_d = 270 cm^{-1}/192 cm^{-1} = 1.41, which is the same as that calculated for the BMA systems, $\mathbf{3a}^+$:$\mathbf{3b}^+$. This indicates that, while slowing the main symmetry breaking vibration leads to a lowering in the HT rate BMH, $\mathbf{4}^+$, the effect is not as pronounced as for BMA cation radical, $\mathbf{3}^+$. Although the existence of this torsional mode is not necessary for HT to occur in $\mathbf{4}^+$, it should influence the HT rate because this vibrational mode affects the instantaneous degree of overlap between the π-orbitals of the chromophores and the bishomocubane bridge orbitals which, in turn, leads to modulation in the magnitude of V_{el} as a trajectory enters the avoided crossing region.

The average value of the energy gap as the trajectories enter the avoided crossing regions is about 0.24 kcal mol^{-1} for $\mathbf{3a}^+$, but is more than 6.5 kcal mol^{-1} for $\mathbf{4a}^+$. Thus a significant fraction of trajectories for $\mathbf{3a}^+$ should undergo surface hopping, whereas most of the trajectories for $\mathbf{4a}^+$ remain on the lower surface. Figure 6 displays histograms of the fraction of trajectories in the ensembles of $\mathbf{3a}^+$ and $\mathbf{3b}^+$, that undergo *n* surface hops *against* the number of surface hops (*n*) that they have undergone (hereafter referred to as 'TSH histograms'). These TSH histograms confirm the above prediction, where approximately 40% of the trajectories for $\mathbf{3a}^+$ undergo surface hopping at least twice. In contrast, 95% of trajectories of $\mathbf{4a}^+$, do not enter the upper surface.

That HT in $\mathbf{3}^+$ is extremely rapid, with about 60% of the trajectories failing to undergo surface hopping, demonstrates that the effect of molecular vibrations outweigh the effect of orbital symmetry for HT processes in $\mathbf{3}^+$.

Turning to the formally symmetry-allowed HT processes in $\mathbf{5}^+$ and $\mathbf{6}^+$, our LZ-TSH model predicts that the frequency of passage for HT in $\mathbf{5}^+$ is 2.1 times greater than for $\mathbf{6}^+$. This prediction is in qualitative agreement with the relative magnitudes of the energy gaps associated with the highest symmetry transition structures for HT ($\Delta E_{ac}(\mathbf{5}^+) = 0.75$ and $\Delta E_{ac}(\mathbf{6}^+) =$ 0.55 kcal mol^{-1}).

The TSH histograms for $\mathbf{5}^+$ and $\mathbf{6}^+$ are displayed in Figure 7 and they show that cation radical $\mathbf{5}^+$ undergoes slightly less surface hops than $\mathbf{6}^+$.

The FT spectrum of ΔE for $\mathbf{5}^+$ is shown in Figure 8. The two main peaks of this spectrum correspond to double bond stretching modes of the CPD rings, the assignments of which were made on the basis of the AM1-CI harmonic frequency calculation carried out on the relaxed, charge-localized ground state. The peaks in the FT spectrum at 1750 and 1576 cm^{-1} correspond, respectively, to the symmetric stretching modes of the neutral and charged CPD units (Figure 9).

There are no obvious symmetry breaking, vibrational modes present in the FT spectrum for $\mathbf{5}^+$, nor are there expected to be, considering the presence of significant electronic coupling in the D_{2d}-symmetry transition structure.

Electron transfer in $\mathbf{5}^-$ is formally symmetry-forbidden, whereas it is symmetry-allowed for $\mathbf{6}^-$. The calculated frequency of passage for $\mathbf{6}^-$ is 3.96 times faster than that calculated for $\mathbf{5}^-$. The TSH histograms for the ensembles of $\mathbf{5}^-$ and $\mathbf{6}^-$ are shown in Figure 10, with more than 60% of trajectories for $\mathbf{5}^-$ entering the upper surface and some hopping up to 12 times. In the case of the anion radical $\mathbf{6}^-$, most trajectories do not enter the upper surface.

Although HT in $\mathbf{7}^+$ and $\mathbf{8}^+$ is symmetry-allowed, the electronic coupling is very weak in both molecules. This is

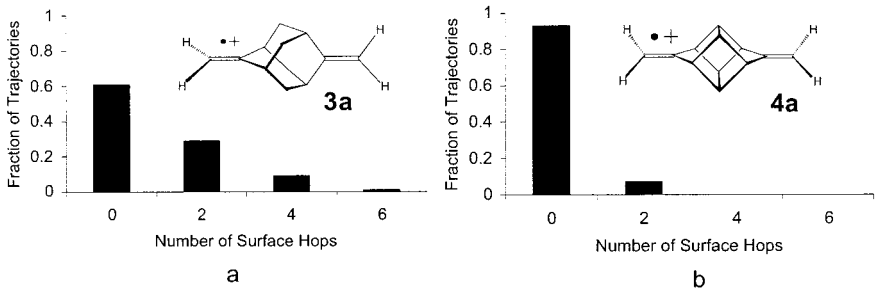

Figure 6. Frequency histograms of the fraction of trajectories in the ensembles of $\mathbf{3a}^+$ (a) and $\mathbf{4b}^+$ (b), that undergo *n* surface hops against the number of surface hops (*n*) that they have undergone.

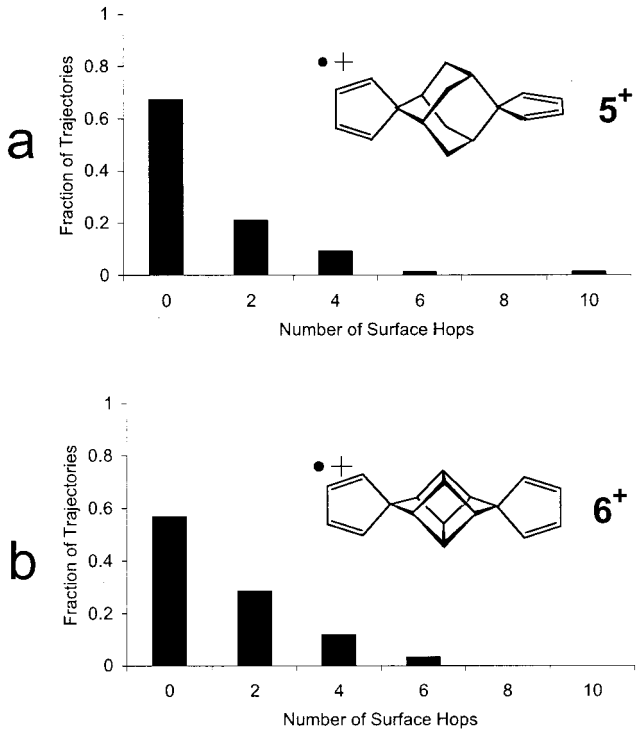

Figure 7. Frequency histograms of the fraction of trajectories in the ensembles of $\mathbf{5}^+$ (a) and $\mathbf{6}^+$ (b), that undergo *n* surface hops against the number of surface hops (*n*) that they have undergone.

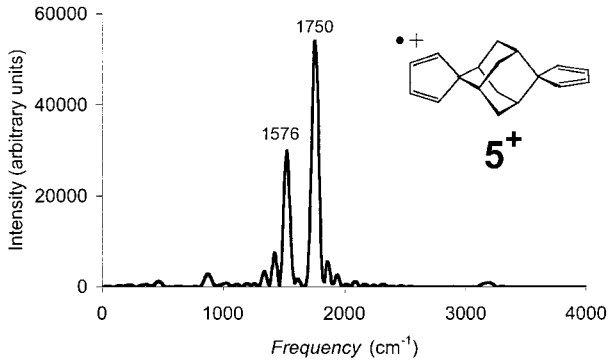

Figure 8. Fourier transform spectrum obtained from the ΔE versus time curve for cation radical $\mathbf{5}^+$, from a trajectory restricted to the reactant well. The two main peaks appear at 1576 and 1750 cm^{-1}.

because the HOMO of the fulvene unit has a nodal plane passing through the exocyclic double bond (see Figure 3b). Consequently, although through-bond interaction, between the HOMOs of the two fulvene units are symmetry-allowed in both **7** and **8**, this mixing is very small owing to the comparatively large through-space distance between the bridge and cyclopentadiene rings. This implies that trajectory surface hopping should

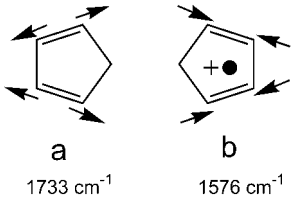

Figure 9. Schematic diagram of the symmetric double bond stretches for the neutral CPD, unit and the charge-localized CPD unit of $\mathbf{5}^+$. These modes drive the HT process.

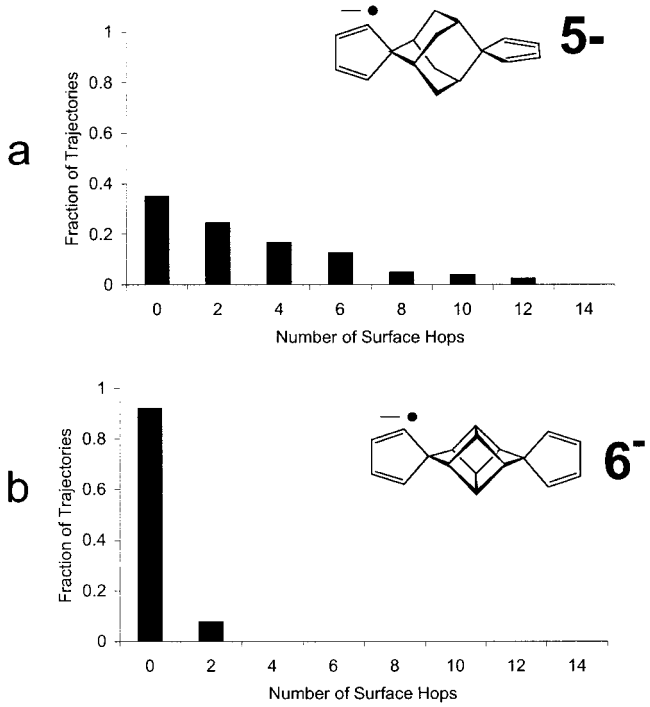

Figure 10. Frequency histograms of the fraction of trajectories in the ensembles of $\mathbf{5}^-$ (a) and $\mathbf{6}^-$ (b), that undergo *n* surface hops *against* the number of surface hops (*n*) that they have undergone.

occur frequently for both $\mathbf{7}^+$ and $\mathbf{8}^+$. The TSH histograms (Figure 11) verify this with 60% of trajectories for each system undergoing at least two surface hops, and a several trajectories for each ensemble undergoing 10 or more surface hops.

The FT spectrum of ΔE for a trajectory of $\mathbf{7}^+$, shown in Figure 12, displays three peaks at 936, 1465, and 1710 cm^{-1}. The two largest peaks, at 1465 and 1710 cm^{-1}, are assigned to the symmetric stretching modes of the hole-localized and neutral CPD units, respectively, and which are similar to those found for $\mathbf{8}^+$ (Figure 9). The peak at 936 cm^{-1} corresponds to "breathing modes" of the adamantane cage which lead to symmetry breaking cage distortions. It is interesting to note that the FT spectrum lacks peaks corresponding to the exocyclic

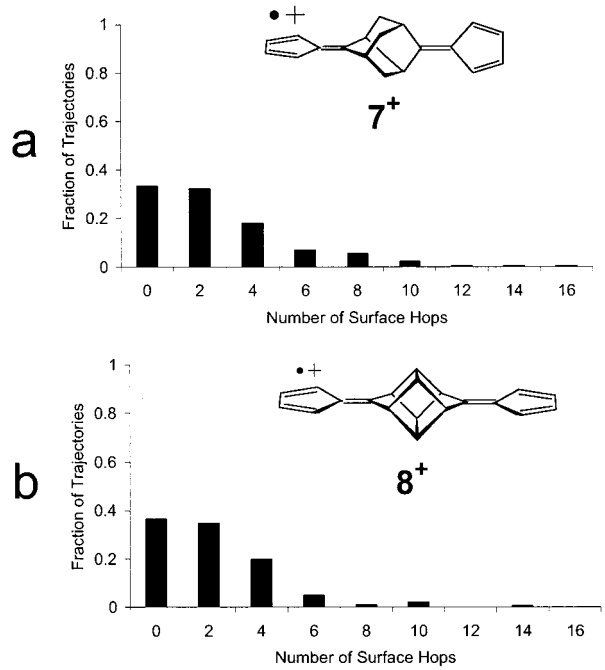

Figure 11. Frequency histograms of the fraction of trajectories in the ensembles of $\mathbf{7}^+$ (a) and $\mathbf{8}^+$ (b), that undergo *n* surface hops *against* the number of surface hops (*n*) that they have undergone.

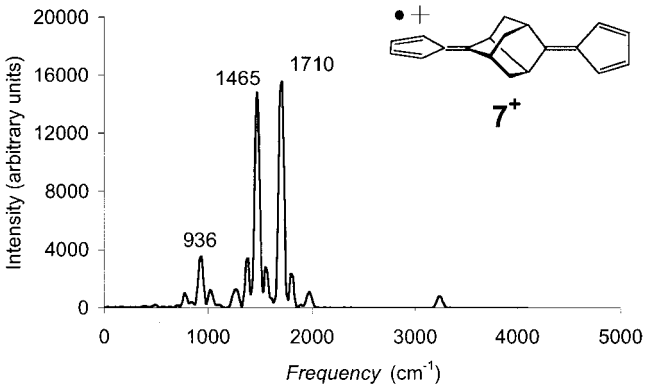

Figure 12. Fourier transform spectrum obtained from a ΔE versus time curve for a trajectory of $\mathbf{7}^+$, which has been restricted to the reactant well.

double bond stretching modes. This is due to the fact that the HOMO's are localized on the CPD units (see Figure 3), and do not extend into the exocyclic double bonds. Consequently, vibrations of the exocyclic double bonds will have minimal influence on the modulation of ΔE.

The frequency of passage for (symmetry-allowed) ET in $\mathbf{8}^-$ is predicted to be 3.4 times greater than that for $\mathbf{7}^-$ where ET is formally symmetry-forbibben Figure 13 displays the TSH histograms for the ensembles of $\mathbf{7}^-$ and $\mathbf{8}^-$.

The histogram shows that in the case of $\mathbf{7}^-$, where ET has an activation barrier of 1.7 kcal mol^{-1} and there is no energy gap at the transition structure of maximum symmetry (D_{2d}), over 70% of the trajectories enter the upper surface at least once. Furthermore, about 35% of the trajectories make multiple hops into the excited state, with about 5% of trajectories surface hopping more than 10 times. Anion radical $\mathbf{8}^-$ has an activation barrier of 2.2 kcal mol^{-1} and an energy gap at the avoided crossing point of maximum symmetry (D_{2h}), of $\Delta E_{ac}(\mathbf{8}^-) = 4.3$ kcal mol^{-1}. Trajectories for $\mathbf{8}^-$, therefore, require a total energy of more than 6.7 kcal mol^{-1} along the reaction coordinate for

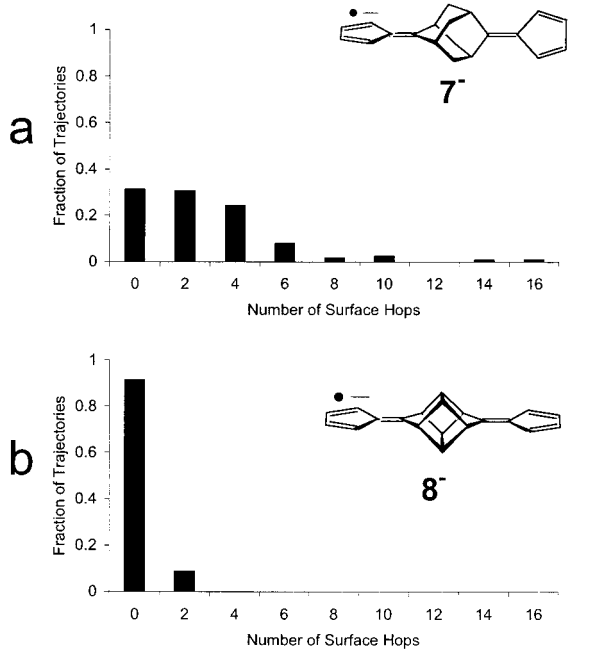

Figure 13. Frequency histograms of the fraction of trajectories in the ensembles of $\mathbf{7}^-$ (a) and $\mathbf{8}^-$ (b), that undergo *n* surface hops *against* the number of surface hops (*n*) that they have undergone.

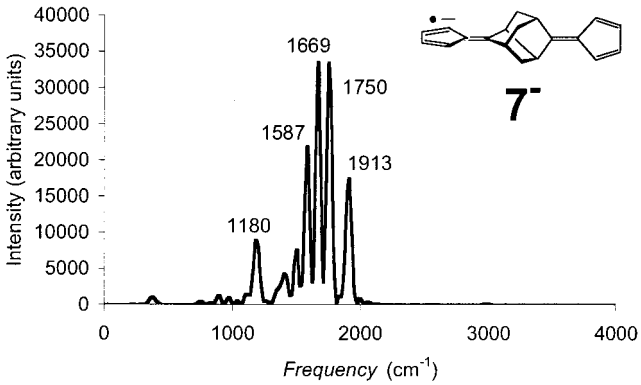

Figure 14. Fourier transform spectrum obtained from a ΔE versus time curve for a trajectory, which is restricted to the reactant well, of $\mathbf{7}^-$.

surface hopping to take place. Indeed, only about 8% of the trajectories for $\mathbf{8}^-$ manage to surface hop.

The FT spectrum of $\mathbf{7}^-$ for a single trajectory reveals some interesting features (Figure 14). In this case, there are five major peaks at 1180, 1587, 1669, 1750, and 1913 cm^{-1}.

The least intense peak (1180 cm^{-1}) corresponds to symmetry-breaking breathing modes of the adamantane cage. The remaining peaks correspond to combinations of various double bond stretching modes and they are depicted in Figure 15. The FT spectrum for $\mathbf{7}^-$ is similar to that for $\mathbf{7}^+$ with the exception that two of the four peaks associated with the double bond stretching vibrations are absent in the FT spectrum of the latter (Figure 12).

The existence of the two extra peaks in the FT spectrum of $\mathbf{7}^-$, and their absence in the FT spectrum of $\mathbf{7}^+$, may be understood from inspection of the HOMOs and LUMOs of BFA, **7**, (see Figures 2 and 3). Because the HOMOs of **7** are restricted to the CPD units of the fulvene chromophores, the vibrations of the exocyclic double bonds have little, if any, influence on modulating the magnitude of the energy gap at the avoided crossing region for the HT reaction in $\mathbf{7}^+$. However, because the LUMOs of the fulvene chromophores in BMA are delocal-

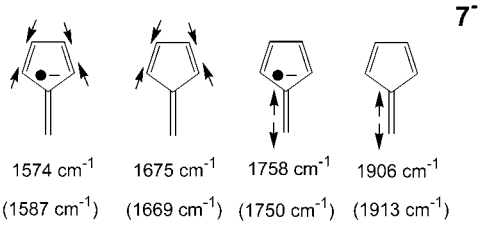

Figure 15. Vibrational modes of $\mathbf{7}^-$ corresponding to the four largest peaks in the FT of Figure 14. Frequencies in brackets are the ones corresponding to the peaks of the FT spectrum. The peaks at 1574 and 1758 cm^{-1} correspond to the charge-localized chromophore.

ized into the exocyclic double bonds, the vibration of these bonds will play a direct role in modulating the energy gap between the electronic states associated with the ET reaction in $\mathbf{7}^-$.

The frequency of passage for ET in $\mathbf{7}^-$ is 4.4 times greater than that for HT $\mathbf{7}^+$, despite the fact that HT in $\mathbf{7}^+$ is symmetry-allowed and ET in $\mathbf{7}^-$ is symmetry-forbidden at their respective D_{2d} symmetry transition states. This interesting result may be understood by once again considering the HOMOs and LUMOs of **7** (Figures 2 and 3), which largely dictate the charge-shift dynamics of HT and ET, respectively. The LUMOs of **7** are delocalized into the exocyclic double bond of each fulvene unit and even extend into the adamantane cage. Symmetry-breaking molecular distortions in **7** should, therefore, allow significant through-bond coupling between the two CPD LUMOs to take place (by way of their mutual overlap with suitable bridge orbitals). In contrast, because of their nodal properties, the two CPD HOMOs couple only weakly with the bridge orbitals and this situation holds irrespective of molecular distortions. Hence, a greater proportion of the trajectories for $\mathbf{7}^+$ might well encounter narrower energy gaps at the avoided crossing region, than for $\mathbf{7}^-$, thereby increasing the number of surface hops and decreasing the overall frequency of passage.

VI. Summary of Results and Overall Analysis of all Systems

This paper details the application of the LZ-TSH model to a series of D−B−A cation and anion radicals, whose charge-delocalized structures have D_{2d} or D_{2h} symmetries. The model is used to analyze HT and ET charge-shift reactions in these systems.

Our model predicts that charge-shift processes occur more slowly in systems where they are formally symmetry-forbidden, compared to their symmetry-allowed counterparts (i.e., $\mathbf{3}^+$ vs $\mathbf{4}^+$, $\mathbf{5}^-$ vs $\mathbf{6}^-$, and $\mathbf{7}^-$, vs $\mathbf{8}^-$). However, the differences in the frequencies of passage between symmetry-forbidden and symmetry-allowed processes are not as large as one might have expected, based on static interpretations of charge transfer processes. The prediction of small symmetry effects on the dynamics of electron and hole transfer processes is supported experimentally. Figure 16 shows such an example where the rate of the symmetry-allowed charge recombination is only slightly faster (2.27×10^7 s^{-1}) in **9**, than the corresponding symmetry-forbidden process in **10** (2.08×10^7 s^{-1}).[13,49]

The LZ-TSH analysis confirms the important role that molecular vibrations play in charge-transfer dynamics and, in particular, their dominance over orbital symmetry effects. By applying Fourier transform techniques and secondary kinetic isotope effects, to reaction trajectories, the main symmetry-breaking vibrations that are responsible for driving the symmetry-forbidden processes were identified.

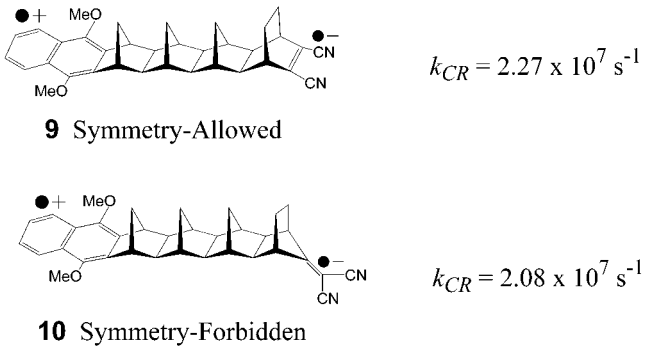

Figure 16. Charge recombination rates for a symmetry-allowed process in system **9**, and a symmetry-forbidden process in system **10**.

The slowest frequencies of passage are calculated for cation radicals $\mathbf{7}^+$ and $\mathbf{8}^+$. Although HT in these systems is formally allowed, electronic coupling in these systems is very small, owing to the nodal properties of the fulvene HOMOs.

Although our LZ-TSH model for studying ET and HT processes appears to provide qualitatively useful insights, it is clearly inappropriate as a general tool for probing charge transfer dynamics. The best way to improve the model, while maintaining the TSH method, is to use Tully's fewest switches algorithm[20] in place of the LZ procedure. We are currently in the process of implementing the Tully algorithm into MOPAC.

Acknowledgment. We thank the Australian Research Council (ARC) for support and for the award of a senior research fellowship to MNP-R. G.A.J. thanks the ARC for a postgraduate scholarship. P.P. acknowledges support from the Department of Energy (DE-FG02-97ER14756). We thank the NSW ac3 and the APAC national facility for a generous allocation of computing time.

Appendix A

The LZ-TSH model involves running individual quasi-classical trajectories on the cation radical or anion radical of interest. Semiempirical molecular orbital (MO) theory, with configuration interaction (CI) between the two active configurations of the charge transfer reaction, is used to calculate the potential energies and energy gradients as the trajectories evolve over the potential energy surface (PES). Surface hopping may occur only at avoided crossings and the Landau−Zener expression (Equation A-1) is used to calculate the probability (P) that a trajectory is to switch adiabatic surfaces

$$P = \exp(-2\pi\gamma)$$

$$\gamma = \frac{V_{el}^{\,2}}{\hbar v |s_1 - s_2|} \qquad \text{(A-1)}$$

Here, V_{el} is the matrix element which couples the diabatic surfaces at the avoided crossing and is equal to half the difference in energy, $\Delta E_{adiabatic}$, between the ground and first excited adiabatic states at this point; v is the velocity of motion along the reaction coordinate at the avoided crossing, and s_1 and s_2 are the first derivatives of the potential energies of the two diabatic states with respect to the reaction coordinate at the avoided crossing. Figure A-1 schematically describes these quantities.There exists a technical detail in the actual calculations used that represents a potential source of confusion with this model. With commonly used MO methods, including those used in MOPAC, employed for the present work, the single-

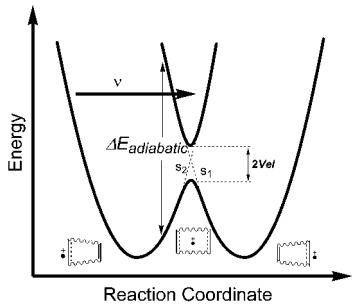

Figure 17. Diagrammatic representation of the parameters required to calculate the Landau−Zener probability of surface hopping at the avoided crossing. Here, v is the velocity of the trajectory in the avoided crossing region, ΔE is the energy gap, and s_1 and s_2 are the slopes of the diabatic surfaces. The position of the excess charge for a hypothetical cation radical diene is shown at the bottom.

configuration wave functions are themselves delocalized. The two adiabatic states (solid curves) in Figure A-1, would be fairly well approximated by such single-configuration delocalized MOs. However, if CI is carried out between the delocalized MOs, the resulting states will be identical to those derived from the CI between diabatic configurations. This fact allows us to retain the description of a crossing between diabatic states in the following text, even though no diabatic wave functions were ever used.

For each of the systems, the distribution of charges associated with the carbon atoms of the chromophores is monitored as a trajectory proceeds. Delocalization of the net charge over the ion's chromophores indicates that the trajectory has entered the avoided crossing region (see bottom of Figure A-1). The parameter Δq is used to monitor the movement of the excess charge of the ion as the trajectory proceeds. It is defined as the sum of the charges of the atoms comprising the donor chromophore *minus* that of the acceptor chromophore

$$\Delta q = \sum_{\substack{\text{donor}\\ \text{atoms}}} q - \sum_{\substack{\text{acceptor}\\ \text{atoms}}} q \qquad \text{(A-2)}$$

Δq is calculated at the beginning of the trajectory (on the ground adiabatic state) and recalculating it for every point along the trajectory (time steps of 0.1 fs are used). Points of the trajectory where Δq changes sign correspond to avoided crossing regions. When this occurs, the probability of surface hopping is calculated at the local point of the trajectory where the adiabatic energy gap, $\Delta E_{\text{adiabatic}}$, is minimum.

At the avoided crossing, the electronic coupling, V_{el}, is simply half the magnitude of the adiabatic energy gap. The other parameters of eq A-1 may be obtained by noting that

$$v|s_1 - s_2| = \frac{d|\Delta E_{\text{diabatic}}|}{dt} \qquad \text{(A-3)}$$

By monitoring the adiabatic states as the trajectory proceeds, $\Delta E_{\text{adiabatic}}$ may be tracked as a function of time. The curvature in $\Delta E_{\text{adiabatic}}(t)$ that arises from configuration mixing as the avoided crossing is approached, ensures that $d|\Delta E_{\text{adiabatic}}|/dt \leq d|\Delta E_{\text{diabatic}}|/dt$ at all points. Consequently, the quantity $d|\Delta E_{\text{diabatic}}|/dt$ is estimated by finding the maximum value of $d|\Delta E_{\text{adiabatic}}|/dt$ as the avoided crossing is approached.

Once the probability of surface hopping has been calculated, a generated pseudo-random number is then interrogated to determine whether the trajectory will undergo surface hopping or not. If so, corrections to the atomic momenta which are required as a result of surface hopping are made using the Miller−George correction factor.[50] If the trajectory is to undergo hopping from the lower to the upper surface and there is insufficient kinetic energy in the reaction coordinate, surface hopping will not occur and the trajectory will continue with its original velocities.

All trajectories are begun in the reactant well as described in Appendix B, and are allowed to run until electron or hole transfer is deemed to occur by relocation of the excess charge to the alternate chromophore. At this point, a trajectory is terminated. A trajectory may undergo surface hopping repeatedly during its lifetime. If charge transfer does not occur within 500 fs the trajectory is terminated and treated as unreactive. The time step used in the simulation is 0.1 fs.

Appendix B

Initialization of the trajectories involved performing harmonic vibrational frequency calculations on the optimized, charge-localized ground-state geometries, for the systems modeled. Separate harmonic frequency calculations were performed for the deuterated systems to account for the isotopic changes to the vibrational frequencies. The procedure for assigning initial velocities and positions is described below.

A canonical ensemble at 298.15 K was generated by quasi-classical normal-mode sampling, using a procedure modified from that of Chapman and Bunker (CB).[30] In the CB method, a harmonic relationship between amplitude and potential energy is assumed for each normal mode, and then corrections for the failures of this relationship that occur with finite displacements from the stationary point are made by an iterative scaling device. In the present procedure, the relationship between displacement and potential energy was fitted to the expression

$$\Delta E_i = \sum_{j=2}^{5} a_{ij}\, \xi_i^j \qquad \text{(B-1)}$$

for the i^{th} normal mode. ΔE_i is the potential energy in excess of the stationary-point value, $\xi^j{}_i$ is the displacement along the direction of the normal coordinate, and the a_{ij} are empirically determined coefficients. For the initial states of each of the trajectories in this study, total potential energy above the stationary point due to simultaneous displacements along all of the normal coordinates was found to be within 1 kcal mol^{-1} of the MOPAC value when calculated by Equation B-1.

The number of quanta in excess of the zero-point was selected for each normal mode by choosing the largest integer, n_i to satisfy relationship B-2

$$n_i \leq -\frac{k_{\text{B}}T}{hc\nu_i}\ln(R_{1i}) \qquad \text{(B-2)}$$

where k_{B} is Boltzmann's constant, h is Planck's constant, c is the speed of light, T is the temperature (here 298.15 K), ν_i is the frequency of i^{th} normal mode (in cm^{-1}), and R_{1i} is a random number in the range $0 \leq R_{1i} \leq 1$.

The energy in each normal mode, $(n_i + 1/2)hc\nu_i$, was converted to a maximum displacement ξ_i by eq B-1, and then the actual displacement, q_i selected by eq 6

$$q_i = \xi_i \cos(2\pi R_{2i}) \qquad \text{(B-3)}$$

where R_{2i} is a second random number in the range $0 \leq R_{2i} \leq 1$. Because the maximum displacements at a given energy were typically not symmetrical in the positive and negative directions

of the normal-coordinate eigenvector, the value appropriate for the sign of eq B-3 was used.

The kinetic energy in each normal mode (the difference between the total energy, $(n_i + 1/2)hc\nu_i$, and the potential energy due to displacement from the stationary point) was used to calculate Cartesian velocity components for each atom, with the directions being selected by a third random number. External molecular rotations were not energized.

The Cartesian atomic coordinates and velocities then formed the input for the dynamic reaction coordinate routine that is part of MOPAC.

References and Notes

(1) Joran, A. D.; Leland, B. A.; Geller, G. G.; Hopfield, J. J.; Dervan, P. B. *J. Am. Chem. Soc.* **1984**, *106*, 6090.

(2) Hush, N. S.; Paddon-Row, M. N.; Cotsaris, E.; H., O.; Verhoeven, J. W.; Heppener, M. *Chem. Phys. Lett.* **1985**, *117*, 8.

(3) Oevering, H.; Paddon-Row, M. N.; Heppener, H.; Oliver, A. M.; Cotsaris, E.; Verhoeven, J. W.; Hush, N. S. *J. Am. Chem. Soc.* **1987**, *109*, 3258.

(4) Johnson, M. D.; Miller, J. R.; Green, N. S.; Closs, G. L. *J. Phys. Chem.* **1989**, *93*, 1173.

(5) Paddon-Row, M. N.; Verhoeven, J. W. *New J. Chem.* **1991**, *15*, 107.

(6) Knapp, S.; Dhar, T. G. M.; Albaneze, J.; Gentemann, S.; Potenza, J. A.; Holten, D.; Schugar, H. J. *J. Am. Chem. Soc.* **1991**, *113*, 4016.

(7) Clayton, A. H. A.; Ghiggino, K. P.; Lawson, J. M.; Paddon-Row, M. N. *J. Photochem. Photobiol. A-Chem.* **1994**, *80*, 323.

(8) Roest, M. R.; Verhoeven, J. W.; Schuddeboom, W.; Warman, J. M.; Lawson, J. M.; Paddon-Row, M. N. *J. Am. Chem. Soc.* **1996**, *118*, 1762.

(9) Calcaterra, L. T.; Closs, G. L.; Miller, J. R. *J. Am. Chem. Soc.* **1983**, *105*, 670.

(10) Miller, J. R.; Calcaterra, L. T.; Closs, G. L. *J. Am. Chem. Soc.* **1984**, *106*, 3047.

(11) Reimers, J. R.; Hush, N. S.; Sammeth, D. M.; Callis, P. R. *Chem. Phys. Lett.* **1990**, *169*, 622.

(12) Zeng, Y.; Zimmt, M. B. *J. Am. Chem. Soc.* **1991**, *113*, 5107.

(13) Oliver, A. M.; Paddon-Row, M. N.; Kroon, J.; Verhoeven, J. W. *Chem. Phys. Lett.* **1992**, *191*, 371.

(14) Paddon-Row, M. N. *Acc. Chem. Res.* **1994**, *27*, 18.

(15) De Cola, L.; Balzani, V.; Barigelletti, F.; Flamigni, L.; Belser, P.; Bernhard, S. *Recl. Trav. Chim. Pays-Bas* **1995**, *114*, 534.

(16) Dantzig, N. A.; Levy, D. H.; Vigo, C.; Piotrowaik, P. *J. Chem. Phys.* **1995**, *103*, 4894.

(17) Yip, W. T.; Levy, D. H.; Kobetic, R.; Piotrowiak, P. *J. Phys. Chem. A* **1999**, *103*, 10.

(18) Landau, L. *Phys. Z. Sowetunion* **1932**, *2*, 46.

(19) Zener, C. *Proc. R. Soc. (London)* **1932**, *A137*, 696.

(20) Tully, J. C. *J. Chem. Phys.* **1990**, *93*, 1061.

(21) Chapman, S. *Adv. Chem. Phys.* **1992**, *82*, 423.

(22) Hack, M. D.; Truhlar, D. G. *J. Phys. Chem.* **2000**, *104*, 7917.

(23) Hack, M. D.; Truhlar, D. G. *J. Chem. Phys.* **2001**, *114*, 2894.

(24) Jones, G. A.; Carpenter, B. K.; Paddon-Row, M. N. *J. Am. Chem. Soc.* **1998**, *120*, 5499.

(25) Jones, G. A.; Carpenter, B. K.; Paddon-Row, M. N. *J. Am. Chem. Soc.* **1999**, *121*, 11 171.

(26) The convention used throughout this paper is that a single structure number is assigned to each molecular structure. For the neutral species there will be no superscript, whereas cation radicals and anion radicals will be denoted by + and − superscripts, respectively.

(27) MOPAC93 ed.; (J. J. P. Stewart and Fuijitsu Limited. Copyright Fugijitsu Limited, Tokyo, Japan), obtainable from QCPE, Department of Chemistry, Indiana University: Bloomington, IN, 47405.

(28) Robb, M. A.; Bernardi, F.; Olivucci, M. *Pure Appl. Chem.* **1995**, *67*, 783.

(29) The frequency of passage (f) is the inverse of the mean first passage time (τ), reported in ref 25. It is incorrect to refer to f as a unimolecular rate constant for CT as the trajectories are not given the opportunity to recross from the product to the reactant well. The model assumes infinitely fast deactivation in the product well.

(30) Chapman, S.; Bunker, D. L. *J. Chem. Phys.* **1975**, *62*, 2890.

(31) Balzani, V.; Barigelletti, F.; Belser, P.; Bernhard, S.; De Cola, L.; Flamigni, L. *J. Phys. Chem.* **1996**, *100*, 16 786.

(32) Paddon-Row, M. N. 2 ed.; Balzani, V., Ed.; Wiley-VCH: Weinheim, 2001; Vol. 3, pp 179−221.

(33) Simmons, H. E.; Fukunaga, T. *J. Am. Chem. Soc.* **1967**, *89*, 5208.

(34) Hoffmann, R.; Imamura, A.; Zeiss, G. D. *J. Am. Chem. Soc.* **1967**, *89*, 5215.

(35) Liu, Y. P.; Lu, D. H.; Gonzalez-Lafont, A.; Truhlar, D. G.; Garrett, B. C. *J. Am. Chem. Soc.* **1993**, *115*, 7806.

(36) Doubleday, C.; Bolton, K.; Peslherbe, G. H.; Hase, W. L. *J. Am. Chem. Soc.* **1996**, *118*, 9922.

(37) Bolton, K.; Hase, W. L.; Peslherbe, G. H. *Modern Methods for Multidimensional Dynamics Computation in Chemistry*; World Scientific: Singapore, 1998.

(38) Martínez-Núñez, E.; Marques, J. M. C.; Vázquez, S. A. *J. Chem. Phys.* **2001**, *115*, 7872.

(39) Salhi-Benachenhou, N.; Engels, B.; Huang, M.; Lunell, S. *Chem. Phys.* **1998**, *236*, 53.

(40) Toriyama, K.; Okazaki, M. *Acta Chem. Scand.* **1997**, *51*, 167.

(41) Toriyama, K.; Okazaki, M. *Appl. Magn. Reson.* **1996**, *11*, 47.

(42) Köppel, H.; Domcke, W.; Cederbaum, L. S.; von Niessen, W. J. *J. Chem. Phys.* **1978**, *69*, 4252.

(43) Merer, A. J.; Schoonveld, L. *Can. J. Phys.* **1969**, *47*, 1731.

(44) Blancafort, L.; Jolibois, F.; Olivucci, M.; Robb, M. A. *J. Am. Chem. Soc.* **2001**, *123*, 722.

(45) Farazdel, A.; Dupuis, M.; Clementi, E.; Aviram, A. *J. Am. Chem. Soc.* **1990**, *112*, 4206.

(46) Reimers, J. R.; Hush, N. S. *Chem. Phys.* **1990**, *146*, 105.

(47) The total kinetic energy assigned to the normal vibrational modes was set to be less than the minimum energy required to access the avoided crossing region. Each vibrational mode was assigned equivalent amounts of kinetic energy (i.e., equal amounts of quanta were assigned to each mode). The restriction of the trajectory to the reactant well is necessary because if the trajectory were allowed to move between the reactant and product wells the resulting FT spectrum becomes complicated, owing to the drastic changes to several of the vibrational force constants that take place upon travelling through the avoided crossing region. Each trajectory was run for 500 fs, with time intervals of 0.1 fs. A Fast Fourier Transform was used, giving a resolution of approximately 20 cm^{-1}.

(48) It must be stressed that this isotope effect is dependent on the ratio of the vibrational frequencies which drive the HT process, rather than on changes in Gibbs free energies of activation which result from differences in zero-point energy between the species. Changes in the Gibbs free energy are not expected to have significant impact on the SKIEs because the vast majority trajectories in this study have sufficient kinetic energy to overcome the activation barrier.

(49) In fact, the systems treated in this manuscript are degenerate and should, therefore, display the largest symmetry effects on electron and hole transfer dynamics. As the energy difference between the donor and acceptor groups increases, significant vibronic coupling will take place, even if the donor is in the formally undistorted vibronic ground state. As a consequence, strongly exergonic charge recombination processes, such as those taking place in **9** (Figure 16), are even less likely to exhibit pronounced symmetry effects. In the case of a degenerate system explicit excitation of the symmetry-breaking mode is necessary.

(50) Miller, W. H.; George, T. F. *J. Chem. Phys.* **1972**, *56*, 5637.